Available online at www.sciencedirect.com

ScienceDirect

journal homepage: www.elsevier.com/locate/he

Effects of injection parameters on propagation patterns of hydrogen-fueled rotating detonation waves

Kepeng Yao [a,d], *Pengfei Yang* [b], *Honghui Teng* [c,*], *Zheng Chen* [b], *Chun Wang* [a,d]

[a] State Key Laboratory of High Temperature Gas Dynamics, Institute of Mechanics, Chinese Academy of Sciences, Beijing 100190, China
[b] SKLTCS, CAPT, College of Engineering, Peking University, Beijing 100871, China
[c] School of Aerospace Engineering, Beijing Institute of Technology, Beijing 100081, China
[d] School of Engineering Sciences, University of Chinese Academy of Sciences, Beijing 100049, China

HIGHLIGHTS

- The effect of injection on rotating detonation waves is quantitatively displayed.
- Increasing slot width can lead to the detonation propagation patterns stably.
- Increasing injection stagnation temperature may lead to a chaotic mode.
- Two parameters are proposed to distinguish the detonation propagation patterns.

GRAPHICAL ABSTRACT

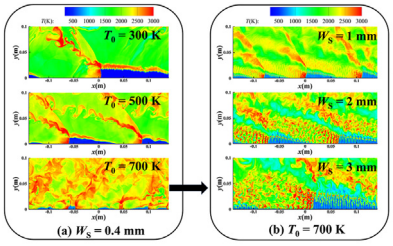

Increasing injection temperature T_0 can increase the number of detonation waves.
Increasing injection slot width W_S can decrease the number of detonation waves.

ARTICLE INFO

Article history:
Received 26 July 2022
Received in revised form
27 August 2022
Accepted 5 September 2022
Available online 26 September 2022

Keywords:
Rotating detonation wave
Incomplete mixing

ABSTRACT

Two-dimensional rotating detonation waves (RDWs) with separate injections of hydrogen and air are simulated using the Navier–Stokes equations together with a detailed chemical mechanism. The effects of injection stagnation temperature and slot width on the detonation propagation patterns are investigated. Results find that extremely high temperatures can lead to a chaotic mode in which detonation waves are generated and extinguished randomly. Increasing the slot width can reduce the number of detonation waves and finally trigger detonation quenching at a low injection stagnation temperature. But increasing the slot width can change the RDW propagation pattern from a chaotic to a stable mode under high injection temperature. Furthermore, the kinetic parameter τ (representing the chemical reactivity of the mixture) and the kinematic parameter α

* *Corresponding author.*
E-mail address: hhteng@bit.edu.cn (H. Teng).
https://doi.org/10.1016/j.ijhydene.2022.09.051

Injection parameters
Propagation pattern

(representing the mixing efficiency of hydrogen and oxygen) are introduced to distinguish the RDW propagation patterns.

Introduction

Detonation is an extreme combustion phenomenon in which the leading shock wave and reaction zone are coupled tightly, and it can propagate at a supersonic speed relative to the unburned gas. As the pressure-gain-combustion [1], engines based on detonation combustion have numerous advantages, such as shorter combustors, higher combustion efficiency, and higher specific impulse. Three types of detonation engines have been proposed and studied widely: the pulse detonation engine (PDE) [2–5], rotating detonation engine (RDE) [6–12], and oblique detonation engine (ODE) [13,14]. The PDE operates in a pulsed mode, whereby the detonation must be initiated in each cycle and fast purging/refilling is required. It is difficult to obtain an oblique detonation wave in the combustor under a low inflow Mach number [15–17]. For the RDE, the rotating detonation wave (RDW) propagates continuously in an annular combustor, thereby avoiding the high-frequency reignition in a PDE [18] and preventing the upstream motion of one detonation wave in an ODE. The RDE has attracted increasing attention in the past decades for its promising application in advanced propulsion [19–23].

The fundamental research of RDWs in simplified combustors has been investigated via theoretical analysis, experimental measurements, and numerical simulations [24–30]. There are many studies on RDW structures under different inflow parameters and geometric configurations. The wave structures in the combustor RDW consist of detonation waves, reactive shock waves, triangular fresh-mixture regions, and contact surfaces. The fuel-injection models of RDE usually include premixed and non-premixed injections. For the premixed injection, the detonation wave height is determined primarily by the stagnation pressure [24,31,32], while the detonation wave number is mainly determined by the stagnation temperature [33,34]. Meanwhile, the detonation wave number for the spacer micro-nozzle injection model is also determined by the injection area ratio [35,36].

The fuel and oxidant are usually injected separately in practice [10,19,23,25,35,37–40]. The mixability of fuel and oxidant can strongly affect the detonation velocity, thrust performance, and detonation wave number in the combustor. Fuel and oxidant must be mixed within one detonation cycle to obtain a stable detonation wave. Poor mixing of the oxidant and fuel decreases the detonation velocity [31,41]. It causes a lower detonation wave velocity compared to the Chapman–Jouguet (CJ) detonation velocity [41–43]. A large injection slot reduces the mixing efficiency, decreases the number of detonation waves [9], and lowers the thrust performance. The thrust performance is also affected by the combustor width, hence, Kawasaki et al. [44] proposed a critical value needed to sustain an RDW in a suitable state for generating thrust.

The aforementioned works have demonstrated that the injection parameters such as injection stagnation temperature/pressure and injection system configuration have an important effect on the combustion mode in the combustor. The stable operation of RDE needs the detonation waves to be initiated and propagated stably in the combustor. However, there are still significant challenges with RDE, including rapidly mixing the reactants and regulating the combustion mode in the combustor. Moreover, the detonation mode is usually regulated by the injection parameters. While there is still lack of quantitative description of the effect on the detonation mode by injection conditions. Therefore, this paper simulated the RDE with a separate injection to study the effect of injection parameters on the detonation mode in the combustor. The generalizing dependences of the detonation wave number on the injection stagnation temperature and slot width are demonstrated in this paper. Two dimensionless parameters are introduced to distinguish the propagation patterns of detonation waves in an RDE combustor, and a criterion is proposed to assess the RDW modes.

Simulation method

Governing equations

The annular RDE combustor has been investigated [23,33,39,45,46]. If the RDE combustor thickness is far smaller than the diameter and the curvature can be ignored, the combustor can be expanded along the bus bar. Similar models have been used in many precious studies [23,31], and the simulated results are consistent with the experiments. Therefore, the computational domain of a three-dimensional combustor is simplified as a rectangular region in this paper. The two-dimensional Navier–Stokes (N–S) equations coupled with detailed reactions are used to simulate the flow field. The N–S equations are written as

$$\frac{\partial \rho}{\partial t}+\frac{\partial \rho u_j}{\partial x_j}=0 \tag{1}$$

$$\frac{\partial \rho u_i}{\partial t}+\frac{\partial \rho u_i u_j+P\delta_{ij}}{\partial x_j}=\frac{\partial \tau_{ij}}{\partial x_j} \tag{2}$$

$$\frac{\partial \rho e}{\partial t}+\frac{\partial \rho u_j e+Pu_j}{\partial x_j}=\frac{\partial \rho u_j \tau_{ij}}{\partial x_j}+\frac{\partial}{\partial x_j}\left(\frac{k\partial T}{\partial x_j}\right)+\frac{\partial}{\partial x_j}\left(\sum_k \rho D h_k \frac{\partial Y_k}{\partial x_j}\right) \tag{3}$$

$$\frac{\partial \rho Y_k}{\partial t}+\frac{\partial \rho Y_k u_j}{\partial x_j}-\frac{\partial}{\partial x_j}\left(\rho D\frac{\partial Y_k}{\partial x_j}\right)=\dot{w}_k \tag{4}$$

with the viscous stress tensor τ_{ij} calculated from

$$\tau_{ij}=\mu\left(\left(\frac{\partial u_i}{\partial x_j}+\frac{\partial u_j}{\partial x_i}\right)-\frac{2}{3}\frac{\partial u_k}{\partial x_k}\delta_{ij}\right) \tag{5}$$

where δ_{ij} is the Kronecker delta. The variables ρ, u_j, e, T, P, Y_k, and h_k are the density, velocity in the j-th direction, specific total energy, temperature, pressure, mass fraction, and enthalpy of the k-th component respectively. The quantity μ is the viscosity, which is calculated from the Sutherland equation, and w_i is the reaction rate of the i-th species, which is calculated from the Arrhenius equation. The diffusion coefficient D is obtained from the Schmidt number and viscosity. The chemical reactions involve multiple components, so the total density and total energy are computed from

$$\rho=\sum_{i=1}^{n}\rho_i \tag{6}$$

$$e=h-\frac{P}{\rho}-\frac{1}{2}\left(u^2+v^2\right) \tag{7}$$

with the enthalpy expressed as

$$h=\sum_{i=1}^{n}\frac{\rho_i h_i}{\rho} \tag{8}$$

where ρ_i is the density of the i-th species, h_i can be solved using the thermodynamic parameters of each independent component, and P is obtained from the state equation

$$P=\sum_{i=1}^{n}\rho_i\frac{R_0}{W_i}T \tag{9}$$

The chemical mechanism of hydrogen-air reaction includes 19 reversible chemical reactions and 9 species (H_2, O_2, H_2O, H, O, OH, HO_2, H_2O_2, and N_2) [47]. The Kurganov–Noelle–Petrova (KNP) scheme [48,49] and the implicit time integration with the forward Euler method are used to solve governing equations, and the Van Leer method [50] is used to calculate numerical flux.

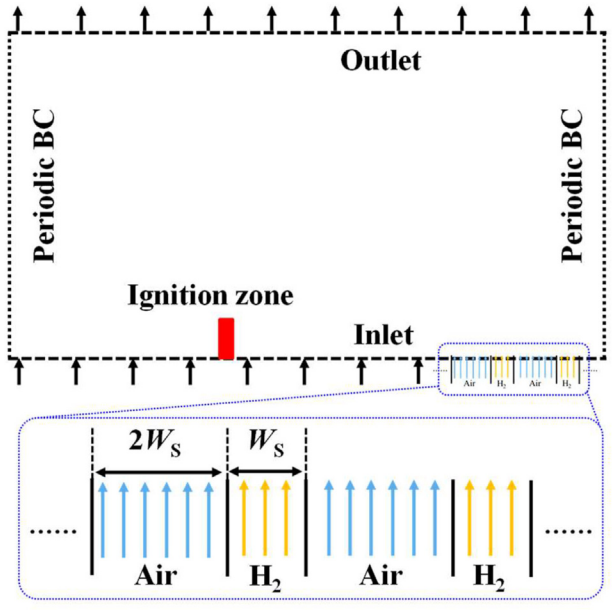

Fig. 1 – Schematic of the computational model.

Physical model

Fig. 1 shows the two-dimensional rectangular domain of a simplified RDE combustor model. In this study, the computational domain size was fixed at 280 mm × 100 mm (the equivalent diameter of the combustor was approximately 90 mm). The left and right boundaries were modeled with periodic boundary conditions. The non-premixed gas (hydrogen/air) was injected axially into the combustor through the sonic nozzle installed separately at the low boundary. The outlet boundary is non-reflective to prevent the interaction between pressure waves and the out boundary. The mixing process of hydrogen and air is sensitive to the injection slot width. To investigate the effect of the mixability of hydrogen and air, this work adjusted the injection width (fuel slot width, W_S) from 0.4 mm to 7.0 mm, and the mixability gradually became worse. Notedly, the area ratio of the oxidant and fuel nozzle was fixed at 2:1, as shown in Fig. 1. The injection stagnation pressure can primarily change the height of the detonation wave but has a slight effect on the detonation wave number [24,31,32]. In this paper, the injection stagnation pressure was set to $P_0 = 1.0$ MPa. The air-breathing RDE can work at a wide Mach number range from 2.0 to 6.0, leading to a remarkable change in the airstream total temperature of the RDE combustor [51]. To explore the effect of injection stagnation temperature T_0 on combustion mode, T_0 changes from 300 K to 700 K, which can ensure the detonation wave can be initiated under low temperature. To initiate the detonation wave, an ignition zone with a high temperature and pressure ($P_{ig} = 3$ MPa, $T_{ig} = 1500$ K, and $U_{ig} = 2000$ m/s) was set in the initial field that was a uniform hydrogen-air mixture with $T = 300$ K and $P = 1.0$ atm.

The flow condition of the inlet nozzle depends on the local pressure P at the combustor entrance. The calculation of inlet parameters can be divided into the following cases [24,33]:

(i) for $P \geq P_0$, the inlet boundary is considered as a wall;
(ii) for $P_0 > P > P_{cr}$, the injection velocity can be obtained from the isentropic expansion

$$T=T_0\left(\frac{P}{P_0}\right)^{\frac{\gamma-1}{\gamma}} \tag{10}$$

$$u=\sqrt{RT_0\frac{2\gamma}{\gamma-1}\left[1-\left(\frac{P}{P_0}\right)^{\frac{\gamma-1}{\gamma}}\right]} \tag{11}$$

where γ and R are the specific heat ratio and the gas constant of the mixture;

(iii) for $P \leq P_{cr}$, the flow is choked, and the injection velocity is sonic.

The critical pressure is defined in terms of the stagnation pressure and specific heat ratio of the reactants as

$$P_{cr} = P_0\left(\frac{2}{\gamma+1}\right)^{\frac{\gamma}{\gamma-1}} \quad (12)$$

Results and discussion

Effects of injection temperature

Fig. 2 shows the temperature contours for different injection stagnation temperatures T_0 and the injection slot width is a constant, i.e., $W_S = 0.4$ mm. The detonation waves are fully developed in all cases. There are three detonation propagation modes, including single-wave mode, dual-wave mode, and chaotic mode. Fig. 2(a) shows the temperature contour when the injection stagnation temperature is $T_0 = 300$ K. The triangular region in the front of the detonation wave is filled with the unburned mixture, and there is only one detonation wave in the combustor. When the injection stagnation temperature is increased to $T_0 = 500$ K, the flow structures are similar to that of $T_0 = 300$ K, including the detonation wave, shock wave, shear layer, and unburned triangular region. However, there are two detonation waves in the combustor, both of which propagate from left to right, as shown in Fig. 2(b). When $T_0 = 700$ K, more small-scale detonation waves propagate in different directions, and the flow field is chaotic, as shown in Fig. 2(c).

To show the flow properties of detonation waves, we extract the pressure and temperature data along the line $y = 0.001$ m in Fig. 2, and the related results are plotted in Fig. 3. From Fig. 3(a) and (b), the pressure and temperature curves are tightly coupled at the wavefront, implying a detonation wave is formed. The rapid pressure drop is due to the heat release and the lateral fluid expansion. The detonation pressure and temperature in Fig. 3(a) and (b) are highly regular when $T_0 = 300$ K and 500 K. However, when T_0 is 700 K, the flow field is in a chaotic state, in which there exist four detonation waves. Meanwhile, two shock waves are also observed and they originated from the collision of two detonation waves, as shown in Fig. 3(c). It should be noted that new detonation waves or shock waves are randomly generated through the hotspot explosion, and the flow fields in Fig. 3(c) are highly unsteady.

A numerical resolution study was conducted to ensure the simulation results were not affected by the grid scales. Fig. 4(a) shows the pressure contours of a flow field in which the RDW

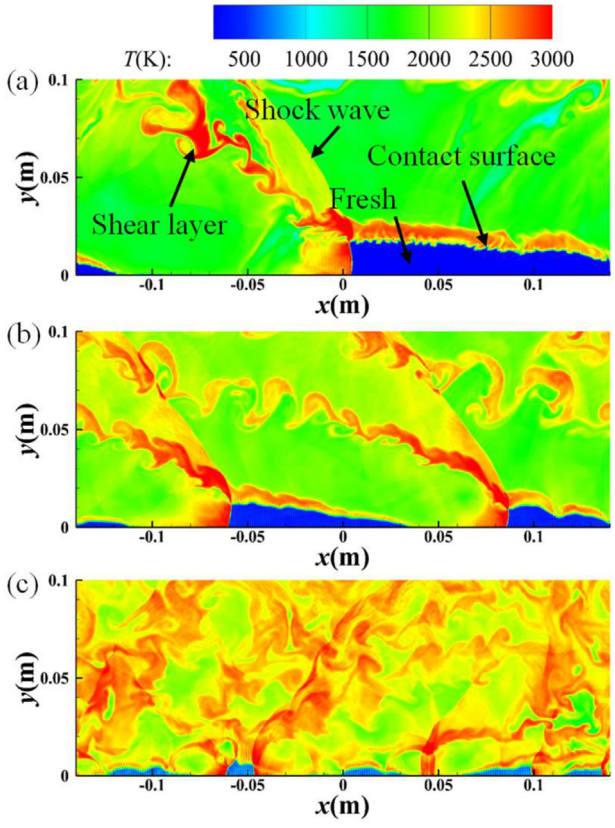

Fig. 2 – Temperature contours for $W_S = 0.4$ mm and $T_0 = 300$ K (a), 500 K (b), and 700 K (c).

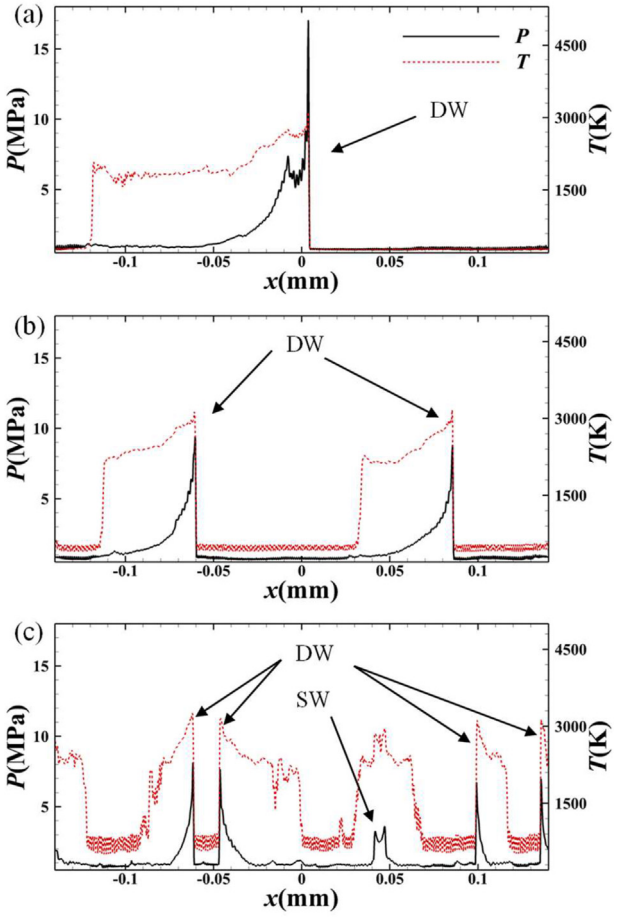

Fig. 3 – Pressure (black solid line) and temperature (red dotted line) distributions along the line $y = 0.001$ m for $W_S = 0.4$ mm and $T_0 = 300$ K (a), 500 K (b), and 700 K (c). SW: shock wave. DW: detonation wave. (For interpretation of the references to color/colour in this figure legend, the reader is referred to the Web version of this article).

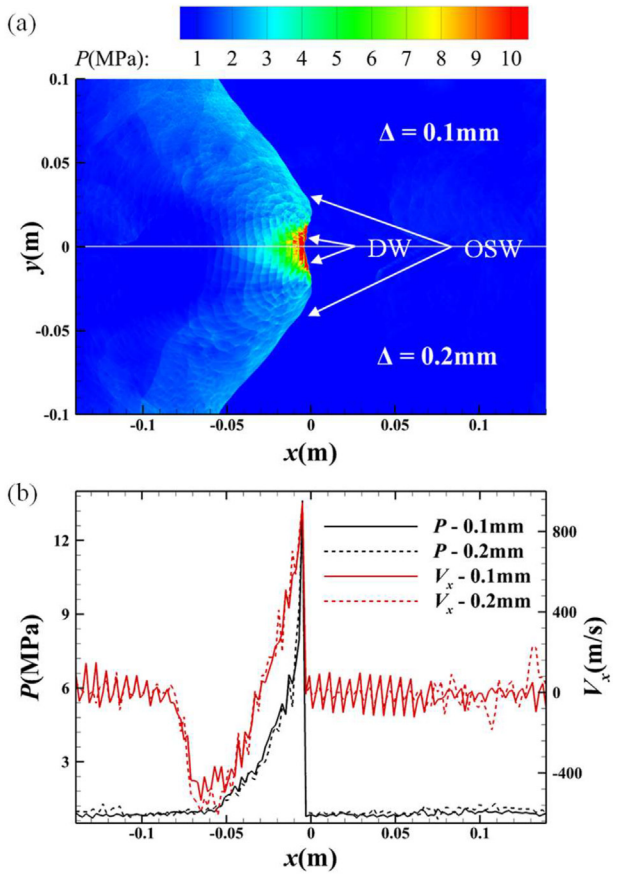

Fig. 4 – Pressure contour (a) and pressure and *x*-velocity distributions along y = 0.005 m (b) of a flow field for W_S = 1 mm and T_0 = 350 K with different grid scales.

runs stably with different resolutions. The mesh widths are Δ = 0.1 mm (upper) and 0.2 mm (lower). The observed flow field structures are similar for different resolutions, and the locations of the detonation waves are almost coincident. For quantitative comparison, the pressure and *x*-velocity distributions of the field near the lower boundary are extracted and plotted in Fig. 4(b). The pressure behind the detonation wave is high, and then it decreases owing to the expansion waves behind the detonation wave. The pressure and *x*-velocity distributions are similar at different resolutions, the detonation wave locations are almost coincident, and the peak pressures and velocities are the same. We conclude that the resolution Δ = 0.2 mm used in this study is sufficient [24,46,52].

Effects of injection slot width

Section 3.1 has demonstrated that the injection stagnation temperature has a great effect on the propagation pattern. Higher injection stagnation temperature leads to more detonation waves in the combustor. If the injection stagnation temperature is higher than a critical value, no stable detonation wave propagates in the combustor, but the detonation waves collide with each other and are extinguished and generated randomly. This is the chaotic combustion mode. Note that the injection slot width in Section 3.1 is 0.4 mm, which can produce a high mixing efficiency flow field and is beneficial to the formation of detonation waves. Now we will discuss the RDE scenario with a high concentration of nonuniformity that is obtained by increasing the injection slot width.

Fig. 5 shows the temperature fields for different injection slot width W_S and the same injection stagnation temperature T_0 = 300 K. When W_S = 1 mm, the flow field does not change significantly compared to the results of Fig. 2(a) where the injection slot width W_S is 0.4 mm. Only one detonation wave is observed in the combustor, but the contact surface between combustion products and fresh mixture is more irregular. When W_S is increased to 2 mm, there is still only one detonation wave in the combustor, and the contact surface is more irregular than for W_S = 1 mm and 0.4 mm. Furthermore, the discrete preignition zones are becoming larger with the increase of slot width. This is due to the lower mixing efficiency of hydrogen and air. A low-temperature region near the shear layer is observed. When W_S is increased to 3 mm, no detonation wave is observed. We can conclude that the larger injection slot is unfavorable to a stable propagation detonation wave when T_0 is only 300 K.

Under a higher injection stagnation temperature, a different phenomenon is observed when W_S is increased. There is a chaotic mode when T_0 = 700 K and W_S = 0.4 mm, as shown in Fig. 2(c). When W_S is increased to 1 mm, three detonation waves are observed in the combustor and propagate in the same direction, as shown in Fig. 6(a). The pressure

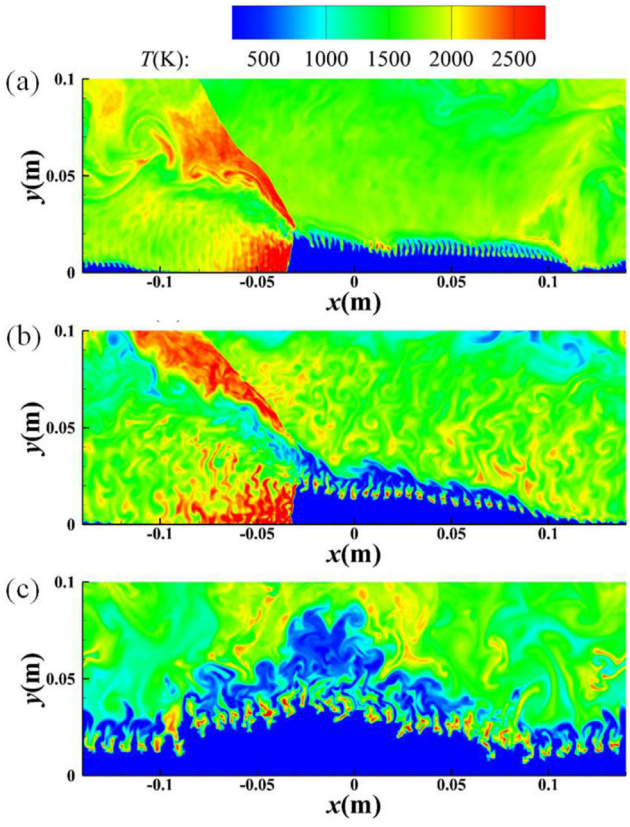

Fig. 5 – Temperature contours for T_0 = 300 K and W_S = 1 mm (a), 2 mm (b), and 3 mm (c).

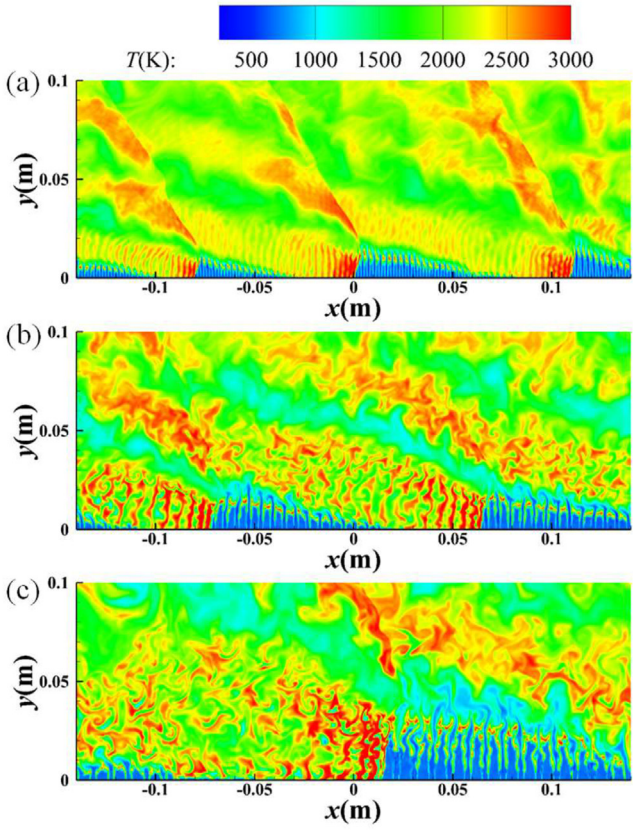

Fig. 6 – Temperature contours for $T_0 = 700$ K and $W_S = 1$ mm (a), 2 mm (b), and 3 mm (c).

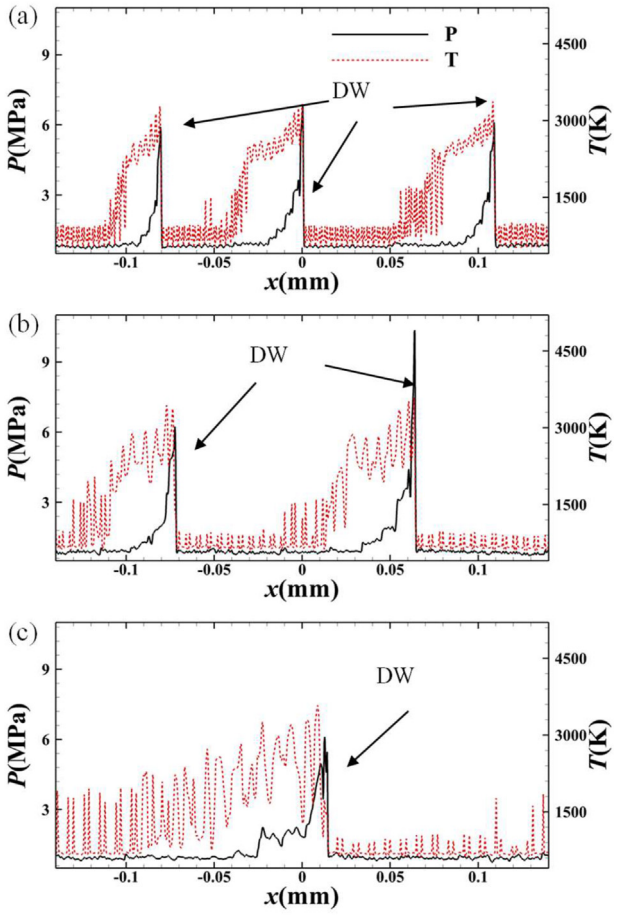

Fig. 7 – Pressure and temperature distributions along the line $y = 0.001$ m for $T_0 = 700$ K and $W_S = 1$ mm (a), 2 mm (b), and 3 mm (c).

and temperature distributions along the line y = 0.001 m are shown in Fig. 7(a). Three stably propagating detonation waves are observed in the combustor, and the temperature distribution oscillates more strongly than for $W_S = 0.4$ mm. Fig. 6(b) shows the temperature contour when W_S is increased to 2 mm. Two detonation waves are observed in the combustor, and spontaneous combustion is observed in the unburned triangular region. Fig. 7(b) shows the pressure and temperature distributions along the line y = 0.001 m. The temperature distribution oscillates more sharply because the hydrogen and air are not mixed as well as with the smaller injection slot, and the reaction takes place at a high temperature in the mixing layer at the contact surface between air and hydrogen. When W_S is increased to 3 mm, only one detonation wave is observed. The height of the detonation wave front is larger than for $W_S = 2$ mm and 1 mm, and spontaneous combustion is observed in the unburned triangular region, as shown in Fig. 6(c). The temperature and pressure oscillate more sharply, as shown in Fig. 7(c). When W_S is increased to 6 mm, no detonation wave is observed in the combustor because no detonation wave can propagate stably, and the field is similar to that in Fig. 5(c).

Comparing the fields in Figs. 5(c) and 6(c) show that increasing the injection stagnation temperature favors stable detonation propagation in the combustor when the injection width is large. From Figs. 2(c) and 6(a), increasing the injection width makes the combustion mode change from chaotic to the stable mode when the injection stagnation temperature is high. It is concluded that increasing temperature benefits stable propagation of the detonation wave but may lead to a chaotic mode. Increasing the injection width is not conducive to stable propagation of the detonation wave when the injection stagnation temperature is low but can change the combustion mode from the chaotic mode to a stable mode when the injection stagnation temperature is higher.

Fig. 8 shows the propagation patterns in the combustor, specifically the number of detonation waves as a function of injection stagnation temperature T_0 when the injection width is $W_S = 0.4$ mm, and as a function of W_S when $T_0 = 700$ K. For $W_S = 0.4$ mm in Fig. 8(a), there is only one detonation wave when $T_0 = 300$ K and 350 K, which we call single-wave mode. When T_0 is increased to 400 K, two detonation waves are observed in the combustor, forming the dual-wave mode. When T_0 is increased to 550 K, there are more detonation waves, which collide with each other and are extinguished, and new detonation waves are generated randomly as in Fig. 2(c), this is the chaotic mode. We can conclude that increasing T_0 leads to more detonation waves in the combustor, and even a chaotic mode when T_0 is higher than a critical value. For $T_0 = 700$ K in Fig. 8(b), the chaotic mode is observed when $W_S = 0.4$ mm. When W_S is increased from 1 mm to 3 mm, the number of detonation waves decreases

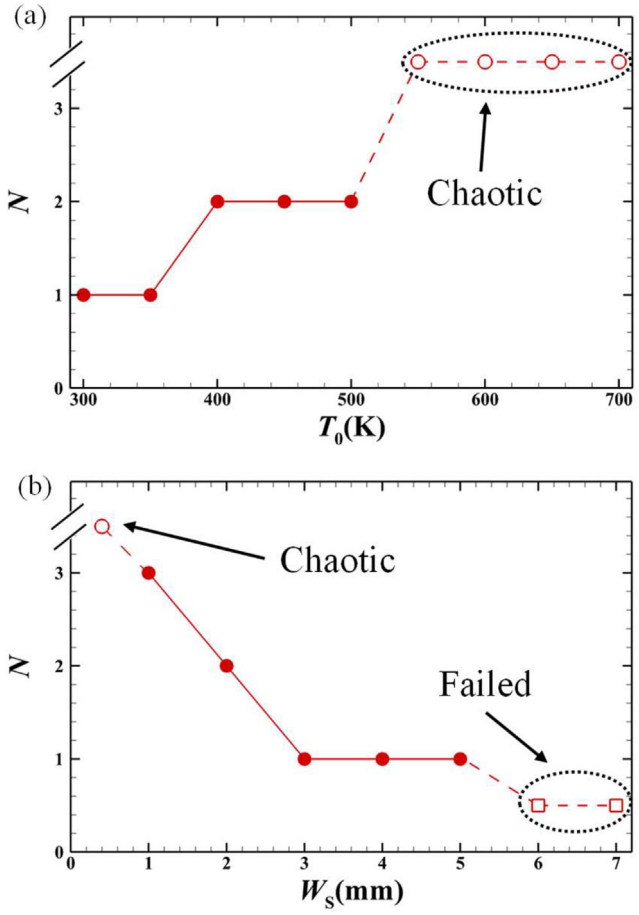

Fig. 8 – Number of detonation waves in the combustor as (a) a function of T_0 when $W_S = 0.4$ mm and (b) a function of W_S when $T_0 = 700$ K.

from three to one. When W_S is increased to 6 mm and 7 mm, no detonation wave is observed, meaning the detonation wave fails to initiate. We can conclude that increasing W_S leads to fewer detonation waves, and even makes a detonation wave unable to propagate in the combustor. From the above, increasing the injection stagnation temperature can lead to a chaotic mode, while increasing the injection width can change the combustion mode from a chaotic to a stable mode but may lead to a failed detonation if the injection width is too large.

Fig. 9 shows the detonation velocity as a function of injection stagnation temperature for $W_S = 1$ mm and 3 mm. The detonation velocity is not constant; that is, the detonation wave has an oscillatory propagation in the combustor. For both $W_S = 1$ mm and 3 mm, the detonation velocity decreases with increasing temperature. From the detonation velocity curves of the two injection widths, the average detonation velocity for $W_S = 1$ mm is higher than for $W_S = 3$ mm for a specific temperature, but the oscillation amplitude of the detonation velocity for $W_S = 1$ mm is smaller than for $W_S = 3$ mm. The reason is that the larger injection slot leads to the hydrogen and air mixing insufficiently. The detonation wave can stably propagate only in the thin mixed layer. Consequently, the propagation of the detonation wave always

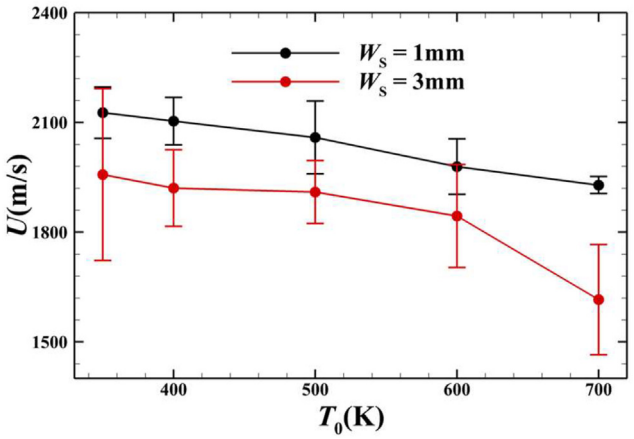

Fig. 9 – Detonation velocity as a function of T_0.

involves quenching and re-initiation, which leads to a larger oscillation amplitude.

Criteria of stable propagation

The injection width and injection stagnation temperature have important effects on the propagation patterns of detonation waves in the combustor. However, the mechanism of these effects is not clear. This section will discuss how injection conditions affect the propagation pattern. The change in injection width has a significant effect on the mixing of the fuel and oxidant, but it has little effect on the chemical reactivity. To explain why increasing injection width changes the propagation pattern from a chaotic to a stable mode, it is necessary to introduce a parameter that represents the mixability of fuel and oxidant to quantify and describe the effect. The kinematic parameter α represents the ratio of the mass fraction $Y_{H_2,reacting}$ of hydrogen that can participate in the reaction (reacting hydrogen) to the total mass fraction of hydrogen in the unburned triangular zone. It is highly related to the equivalence ratio in the combustion theory foundation, but it can visually represent the ratio of the mass fraction of combustible hydrogen due to high concentration non-uniformity.

$$\alpha = \frac{\sum_{i=1}^{n}\left(Y_{H_2,reacting,i} \times \rho_i\right)}{\sum_{i=1}^{n}\rho_{H_2,i}} \tag{13}$$

where

$$Y_{H_2,reacting} = \min\left(Y_{H_2}, Y_{O_2} \cdot \frac{2M_{H_2}}{M_{O_2}}\right) \tag{14}$$

where, the variables Y_{H_2}, Y_{O_2}, M_{H_2}, M_{O_2}, ρ_i and $\rho_{H_2,i}$ are mass fraction, mole mass of hydrogen and oxygen, the total density of field, and fractional density of hydrogen at i-point. Respectively.

Fig. 10 shows the mass fraction distribution of reacting hydrogen $Y_{H_2,reacting}$, for $T_0 = 300$ K with different W_S. The results suggest that the reacting hydrogen in the unburned triangular zone is well distributed for $W_S = 0.4$ mm, which means the mixability of hydrogen and oxygen is sufficient.

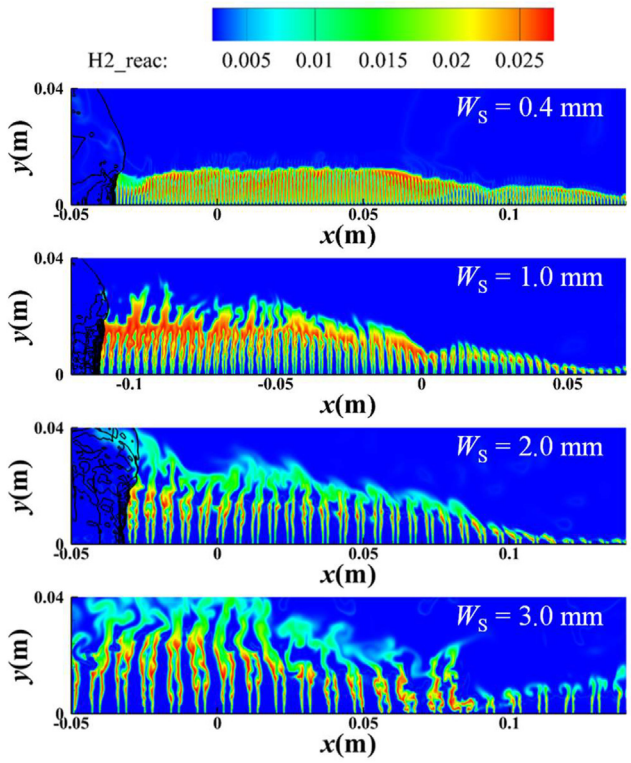

Fig. 10 – Mass fraction distributions of reacting H_2 for different values of W_S at T_0 = 300 K. The black lines are pressure contours representing the detonation waves and shock wave surfaces.

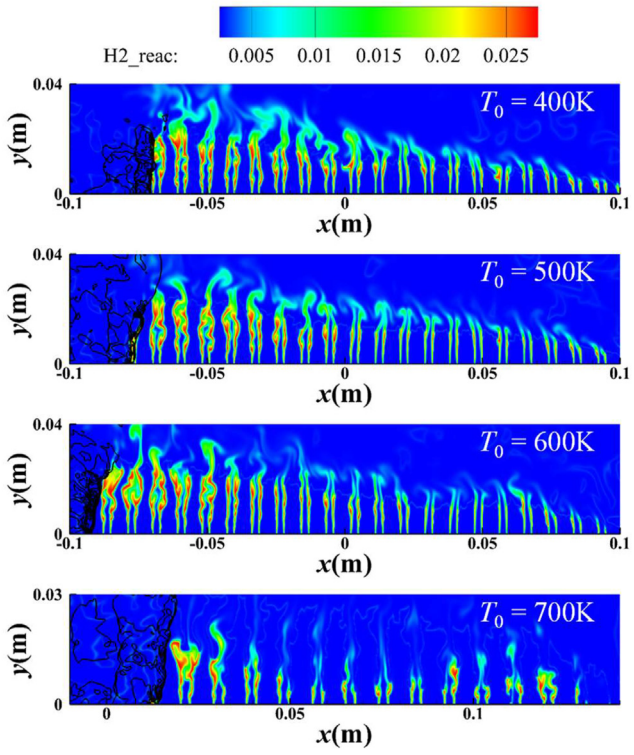

Fig. 11 – Mass fraction distributions of reacting H_2 for W_S = 3 mm at different injection stagnation temperatures. The black lines are pressure contours representing the detonation waves and shock wave surfaces.

However, the reacting hydrogen distribution when $W_S = 1.0$ mm is less homogeneous than when $W_S = 0.4$ mm. If W_S continues increasing to 2.0 mm, there is a larger reacting hydrogen free zone between two reacting hydrogen zones, which means there is less reacting hydrogen, and its distribution is less homogeneous. For W_S = 3 mm, the reacting hydrogen free zone is larger, and no detonation wave is observed from Fig. 5(c). Qualitatively, the reacting hydrogen distribution is less homogeneous as the injection width W_S increases. This means the mixing of hydrogen and oxygen is insufficient, which heavily influences detonation wave propagation. For W_S = 0.4 mm, the detonation wave propagates relatively stable in the well-distributed combustible gas. However, for $W_S = 1$ mm and 2 mm, the propagation process is like that of a normal detonation wave propagating in an inhomogeneous gas mixture, first passing through the inert gas layer and then the combustible gas layer. Therefore, the propagation of a detonation wave always involves re-initiation and quenching. For a larger injection width, the reacting hydrogen-free zone is larger, and the detonation wave cannot propagate in this field because the incombustible gas zone is now too large [53,54].

Fig. 11 shows the mass fraction distributions of reacting hydrogen for $W_S = 3$ mm with different T_0. The results suggest that the reacting hydrogen distribution in the unburned triangular zone does not change significantly as T_0 increases from 400 K to 600 K, which means the width of the incombustible zones (containing only oxygen or hydrogen) has little change. However, for T_0 = 700 K, the reacting hydrogen decreases heavily because the combustible gas in the mixing layer spontaneously combusts. We conclude that the reacting hydrogen distribution is insensitive to the injection stagnation temperature T_0 when there is no spontaneous combustion.

Increasing T_0 favors initiation and stable propagation of detonation waves, even leading to a chaotic mode. However, Fig. 11 shows that increasing T_0 has little effect on the mixing of hydrogen and oxygen. Increasing the combustible gas temperature generally increases the chemical reactivity of the combustible gas. Therefore, quantifying the effect of injection stagnation temperature requires introducing another parameter to represent the chemical reactivity of the mixture in the unburned triangular zone. The kinetic parameter τ is introduced and defined as

$$\tau^{-1} = \frac{\tau_I}{\tau_R} \tag{15}$$

where τ_I and τ_R represent the induction delay time and exothermic delay time of a ZND detonation wave in an unburned triangular zone respectively. The induction time and the exothermic time are usually used to evaluate the detonation instabilities that have a huge influence on detonation combustion [55]. Since the incomplete mixing under the

condition of non-premixed injection, we first calculate the one-dimensional ZND detonation wave, and its averaged temperature/pressure and equivalence ratio are obtained by considering the density-weighted method.

$$\overline{T}=\frac{\sum_{i=1}^{n}\left(T_i\times\rho_{H_2,reacting,i}\right)}{\sum_{i=1}^{n}\rho_{H_2,reacting,i}},\ \overline{p}=\frac{\sum_{i=1}^{n}\left(p_i\times\rho_{H_2,reacting,i}\right)}{\sum_{i=1}^{n}\rho_{H_2,reacting,i}},\ \overline{\varphi}=\frac{\sum_{i=1}^{n}\frac{\rho_{H_2,i}}{M_{H_2}}}{2\cdot\sum_{i=1}^{n}\frac{\rho_{O_2,i}}{M_{O_2}}} \quad (16)$$

Fig. 12 shows the parameters α and τ as functions of injection width W_S and injection stagnation temperature T_0. The black and red curves in Fig. 12(a) show the trends of the kinematic parameter α and kinetic parameter τ with injection width W_S respectively. The black curve drops with increasing W_S, but the red curve is horizontal. For $T_0 = 300$ K, the kinematic parameter α decreases with increasing injection width, but the kinetic parameter τ changes little. In contrast, for $W_S = 3$ mm, τ increases with increasing injection stagnation temperature. The kinematic parameter α is largely unchanged when the injection stagnation temperature increases from 300 K to 600 K, but decreases when T_0 increases to 700 K because of the spontaneous combustion in the unburned triangular zone. We can conclude that increasing the injection width decreases the kinematic parameter α, which means the mixing of hydrogen and oxygen is less sufficient. Therefore, increasing the injection width hampers detonation wave propagation. However, increasing the injection stagnation temperature increases the kinetic parameter τ, which means the chemical reactivity of the mixture is enhanced. That is, increasing the injection stagnation temperature favors initiation and stable propagation of a detonation wave, even leading to a chaotic mode in the combustor.

This study conducted further simulations to study the relations between detonation wave patterns and injection stagnation temperature and injection width. We propose a criterion to predict the propagation pattern to make it easy to regulate and control combustion in the combustor. Fig. 13 shows three kinds of propagation patterns plotted in terms of the parameters α and τ. Two critical curves demarcate the section of stable propagation of the detonation wave in the combustor. We observe that there are two critical values of α for a specific value of τ. These are the initiation critical value α_{cri} and chaotic combustion critical value α_{crc}. When $\alpha < \alpha_{cri}$, no detonation wave is observed in the combustor, which means the detonation wave fails to initiate, and the flow field is like that in Fig. 5(c). When $\alpha > \alpha_{crc}$, the chaotic mode is observed in the combustor, as in Fig. 2 (c). One or more detonation waves propagate stably in the combustor when $\alpha_{cri} < \alpha < \alpha_{crc}$. This is an ideal RDE combustion state. In addition, α_{cri} decreases with increasing τ, but the decrease is not sharp. The upper threshold α_{crc} also decreases with increasing τ, but the decrease is sharp. Notably, only for a higher τ, the chaotic combustion critical value α_{crc} exists. This means there will be no chaotic mode in the combustor even for large α when τ is too small.

In summary, the chemical reactivity and mixability are denoted by the kinematic parameter α and kinetic parameter τ. The mixability of air and hydrogen is dominated by the

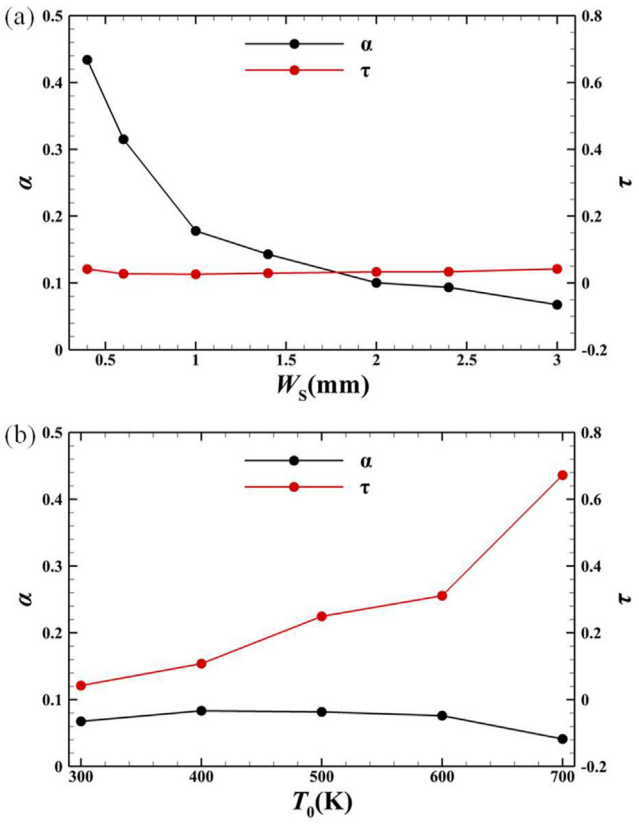

Fig. 12 – α and τ as functions of (a) W_S at $T_0 = 300$ K and (b) T_0 at $W_S = 3$ mm.

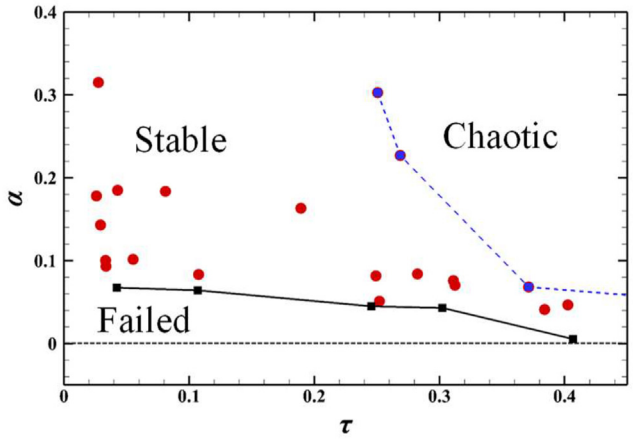

Fig. 13 – Critical condition for stable detonation propagation.

injection slot width, while the chemical reactivity is sensitive to the temperature. Increases the injection slot width, the hydrogen and air mixing more insufficiently, which leads to the α decrease. The kinetic parameter τ increases with the stagnation temperature, while is insensitive to the injection slot width. Under a higher τ (higher chemical reactivity), the detonation cannot be initiated when the mixability is too insufficient. While spontaneous combustion will be observed

when the mixability is sufficient. The stable detonation mode is observed only when mixability is median. Similarly, with increases of τ, the detonation propagation mode goes through the stage of failed detonation, stable propagation, and chaotic mode.

Conclusion

Using a detailed hydrogen/air reaction model together with the N–S equations, two-dimensional rotating detonation combustors with separate injection slots are simulated numerically. The injection stagnation temperature and slot width were adjusted to examine the effects of chemical reactivity and mixing efficiency on RDW propagation patterns.

Results show that the detonation propagation pattern is dominated by the injection stagnation temperature and slot width. Increasing injection temperature can increase the number of detonation waves. The chaotic mode is observed when the slot width is smaller than a critical value under a high stagnation temperature. Increasing the slot width can change the detonation propagation pattern from the chaotic to stable mode, and even quench the detonation. It is because the hydrogen and air in the unburned triangular zone are inhomogeneous. When the injection width is too large, the mixing of hydrogen and oxygen will become highly insufficient, and the fuel-rich and fuel-lean zones exit in turn in the triangular zone. The detonation wave cannot propagate in a zone that only has fuel or oxidant, so no detonation wave is observed. However, a higher injection stagnation temperature is more beneficial to the reaction of the fresh mixture and improves the detonation limits under the non-uniform scenario. Hence, the detonation waves have been again observed even for large slot widths. But extremely high temperature probably causes a chaotic mode, in which detonation waves are generated randomly by the local explosion.

Furthermore, this paper introduced two non-dimensional parameters, the kinetic parameter τ and kinematic α, which represent the chemical reactivity of the mixture and the mixing efficiency of hydrogen and oxygen, respectively. The $\tau-\alpha$ plane is divided into three sections: a failed detonation zone, a stable detonation zone, and a chaotic combustion zone. There are two critical values α_{cri} and α_{crc} for a specific τ. No significant detonation wave is initiated for $\alpha < \alpha_{cri}$, while a chaotic RDW mode can be observed for $\alpha > \alpha_{crc}$. A stable single-wave or dual-wave detonation occurs only when $\alpha_{cri} < \alpha < \alpha_{crc}$. Notably, the chaotic mode is only observed in high chemical reactivity. There will be no chaotic mode even for large α if τ is too small. In other words, it is not conducive to the stable propagation of detonation wave for both too insufficient and sufficient mixing under a high chemical reactivity. The propagation patterns can be forecasted and controlled using the injection width and stagnation temperature.

Declaration of competing interest

The authors declare that they have no known competing financial interests or personal relationships that could have appeared to influence the work reported in this paper.

Acknowledgments

This research was supported by the National Natural Science Foundation of China (NSFC, Nos. 12202014, 12002041 and 11822202) and the China Postdoctoral Science Foundation (No. 2021M700222). The authors thank Dr. Cheng Tian from the Beijing Institute of Technology for assistance with developing the in-house codes.

REFERENCES

[1] Wolański P. Detonative propulsion. Proc Combust Inst 2013;34:125–58. https://doi.org/10.1016/j.proci.2012.10.005.
[2] Jackson SI, Shepherd JE. Toroidal imploding detonation wave initiator for pulse detonation engines. AIAA J 2007;45:257–70. https://doi.org/10.2514/1.24662.
[3] Kailasanath K, Patnaik G. Performance estimates of pulsed detonation engines. Proc Combust Inst 2000;28:595–601. https://doi.org/10.1016/S0082-0784(00)80259-3.
[4] Zhu R, Fang X, Xu C, Zhao M, Zhang H, Davy M. Pulsating one-dimensional detonation in ammonia-hydrogen–air mixtures. Int J Hydrogen Energy 2022;47:21517–36. https://doi.org/10.1016/j.ijhydene.2022.04.265.
[5] Dai T, Zhang B, Liu H. On the explosion characteristics for central and end-wall ignition in hydrogen-air mixtures: a comparative study. Int J Hydrogen Energy 2021;46:30861–9. https://doi.org/10.1016/j.ijhydene.2021.06.213.
[6] Ma Y, Zhou S, Ma H, Ge G, Yu D, Zou G, Liang Z, Zhang T. Experimental investigation on propagation characteristics of liquid-fuel/preheated-air rotating detonation wave. Int J Hydrogen Energy 2022;47:24080–92. https://doi.org/10.1016/j.ijhydene.2022.05.186.
[7] Yokoo R, Goto K, Kim J, Kawasaki A, Matsuoka K, Kasahara J, Matsuo A, Funaki I. Propulsion performance of cylindrical rotating detonation engine. AIAA J 2020;58:5107–16. https://doi.org/10.2514/1.J058322.
[8] Meng Q, Zhao N, Zhang H. On the distributions of fuel droplets and in situ vapor in rotating detonation combustion with prevaporized n-heptane sprays. Phys Fluids 2021;33. https://doi.org/10.1063/5.0045222.
[9] Frolov SM, Aksenov VS, Ivanov VS, Shamshin IO. Large-scale hydrogen–air continuous detonation combustor. Int J Hydrogen Energy 2015;40:1616–23. https://doi.org/10.1016/j.ijhydene.2014.11.112.
[10] Salvadori M, Tudisco P, Ranjan D, Menon S. Numerical investigation of mass flow rate effects on multiplicity of detonation waves within a h2/air rotating detonation combustor. Int J Hydrogen Energy 2022;47:4155–70. https://doi.org/10.1016/j.ijhydene.2021.10.270.
[11] Xia Z, Ma H, He Y, Ge G, Zhou C. Low frequency instability in a h2/air plane-radial rotating detonation engine. Int J Hydrogen Energy 2022;47:5663–76. https://doi.org/10.1016/j.ijhydene.2021.11.175.
[12] Xia Z, Ma H, Ge G, Zhou C. Visual experimental investigation on initiation process of H2/air rotating detonation wave in plane-radial structure. Int J Hydrogen Energy 2020;45:29579–93. https://doi.org/10.1016/j.ijhydene.2020.07.257.
[13] Jiang Z, Zhang Z, Liu Y, Wang C, Luo C. The criteria for hypersonic airbreathing propulsion and its experimental verification. Chin J Aeronaut 2020;34:94–104. https://doi.org/10.1016/j.cja.2020.11.001.
[14] Rosato DA, Thornton M, Sosa J, Bachman C, Goodwin GB, Ahmed KA. Stabilized detonation for hypersonic propulsion.

P Natl Acad Sci USA 2021;118:e2102244118. https://doi.org/10.1073/pnas.2102244118.
[15] Zhang Z, Wen C, Zhang W, Liu Y, Jiang Z. Formation of stabilized oblique detonation waves in a combustor. Combust Flame 2021;223:423–36. https://doi.org/10.1016/j.combustflame.2020.09.034.
[16] Qin Q, Zhang X. Nitrogen dilution effects on the local detachment of the oblique detonation wave in the 2H2–O2 mixture. Int J Hydrogen Energy 2021;46:6873–84. https://doi.org/10.1016/j.ijhydene.2020.11.157.
[17] Qin Q, Zhang X. Controllable initiation characteristics of the oblique detonation wave in a combustor with a confined cone of a novel structure. Aero Sci Technol 2020;107:106267. https://doi.org/10.1016/j.ast.2020.106267.
[18] Anand V, Gutmark E. Rotating detonation combustors and their similarities to rocket instabilities. Prog Energ Combust 2019;73:182–234. https://doi.org/10.1016/j.pecs.2019.04.001.
[19] Sun J, Zhou J, Liu S, Lin Z, Lin W. Numerical investigation of a non-premixed hollow rotating detonation engine. Int J Hydrogen Energy 2019;44:17084–94. https://doi.org/10.1016/j.ijhydene.2019.04.168.
[20] Wu D, Liu Y, Liu Y, Wang J. Numerical investigations of the restabilization of hydrogen–air rotating detonation engines. Int J Hydrogen Energy 2014;39:15803–9. https://doi.org/10.1016/j.ijhydene.2014.07.159.
[21] Lin W, Shi Q, Liu S, Lin Z, Tong Y, Su L, Nie W. Study of thrust vector control for the rotating detonation model engine. Int J Hydrogen Energy 2022;47:1292–305. https://doi.org/10.1016/j.ijhydene.2021.10.050.
[22] Metrow C, Gray S, Ciccarelli G. Detonation propagation through a nonuniform layer of hydrogen-oxygen in a narrow channel. Int J Hydrogen Energy 2021;46:21726–38. https://doi.org/10.1016/j.ijhydene.2021.03.221.
[23] Zhao M, Cleary MJ, Zhang H. Combustion mode and wave multiplicity in rotating detonative combustion with separate reactant injection. Combust Flame 2021;225:291–304. https://doi.org/10.1016/j.combustflame.2020.11.001.
[24] Schwer D, Kailasanath K. Numerical investigation of the physics of rotating-detonation-engines. Proc Combust Inst 2011;33:2195–202. https://doi.org/10.1016/j.proci.2010.07.050.
[25] Bykovskii FA, Vedernikov EF. Continuous detonation combustion of an annular gas-mixture layer. Combust Explo Shock+ 1996;32:489–91. https://doi.org/10.1007/Bf01998570.
[26] Katta VR, Cho KY, Hoke JL, Codoni JR, Schauer FR, Roquemore WM. Effect of increasing channel width on the structure of rotating detonation wave. Proc Combust Inst 2019;37:3575–83. https://doi.org/10.1016/j.proci.2018.05.072.
[27] Deng L, Ma H, Xu C, Liu X, Zhou C. The feasibility of mode control in rotating detonation engine. Appl Therm Eng 2018;129:1538–50. https://doi.org/10.1016/j.applthermaleng.2017.10.146.
[28] Zhou S, Ma H, Zhou C, Hu N. Experimental research on the propagation process of rotating detonation wave with a gaseous hydrocarbon mixture fuel. Acta Astronaut 2021;179:1–10. https://doi.org/10.1016/j.actaastro.2020.10.027.
[29] Pan J, Dong S, Wei H, Li T, Shu G, Zhou L. Temperature gradient induced detonation development inside and outside a hotspot for different fuels. Combust Flame 2019;205:269–77. https://doi.org/10.1016/j.combustflame.2019.04.003.
[30] Pan J, Wang L, He Y, Wei H, Shu G, Li T. Hotspot auto-ignition induced detonation development: emphasis on energy density and chemical reactivity. Combust Theor Model 2021;26:179–200. https://doi.org/10.1080/13647830.2021.1996635.
[31] Tsuboi N, Watanabe Y, Kojima T, Hayashi AK. Numerical estimation of the thrust performance on a rotating detonation engine for a hydrogen–oxygen mixture. Proc Combust Inst 2015;35:2005–13. https://doi.org/10.1016/j.proci.2014.09.010.
[32] Liu Y, Zhou W, Yang Y, Liu Z, Wang J. Numerical study on the instabilities in h2-air rotating detonation engines. Phys Fluids 2018;30:046106. https://doi.org/10.1063/1.5024867.
[33] Yan C, Teng H, Ng HD. Effects of slot injection on detonation wavelet characteristics in a rotating detonation engine. Acta Astronaut 2021;182:274–85. https://doi.org/10.1016/j.actaastro.2021.02.010.
[34] Teng H, Zhou L, Yang P, Jiang Z. Numerical investigation of wavelet features in rotating detonations with a two-step induction-reaction model. Int J Hydrogen Energy 2020;45:4991–5001. https://doi.org/10.1016/j.ijhydene.2019.12.063.
[35] Yao S, Tang X, Luan M, Wang J. Numerical study of hollow rotating detonation engine with different fuel injection area ratios. Proc Combust Inst 2017;36:2649–55. https://doi.org/10.1016/j.proci.2016.07.126.
[36] Zhao M, Zhang H. Origin and chaotic propagation of multiple rotating detonation waves in hydrogen/air mixtures. Fuel 2020;275:117986. https://doi.org/10.1016/j.fuel.2020.117986.
[37] Bykovskii FA, Zhdan SA, Vedernikov EF. Continuous spin detonations. J Propul Power 2006;22:1204–16. https://doi.org/10.2514/1.17656.
[38] Kindracki J, Wolański P, Gut Z. Experimental research on the rotating detonation in gaseous fuels–oxygen mixtures. Shock Waves 2011;21:75–84. https://doi.org/10.1007/s00193-011-0298-y.
[39] Walters IV, Gejji RM, Heister SD, Slabaugh CD. Flow and performance analysis of a natural gas-air rotating detonation engine with high-speed velocimetry. Combust Flame 2021;232:111549. https://doi.org/10.1016/j.combustflame.2021.111549.
[40] Sun B, Ma H. Two-dimensional numerical study of two-phase rotating detonation wave with different injections. AIP Adv 2019;9. https://doi.org/10.1063/1.5113881.
[41] Fujii J, Kumazawa Y, Matsuo A, Nakagami S, Matsuoka K, Kasahara J. Numerical investigation on detonation velocity in rotating detonation engine chamber. Proc Combust Inst 2017;36:2665–72. https://doi.org/10.1016/j.proci.2016.06.155.
[42] Wang Y, Wang J. Effect of equivalence ratio on the velocity of rotating detonation. Int J Hydrogen Energy 2015;40:7949–55. https://doi.org/10.1016/j.ijhydene.2015.04.072.
[43] Nakagami S, Matsuoka K, Kasahara J, Matsuo A, Funaki I. Experimental study of the structure of forward-tilting rotating detonation waves and highly maintained combustion chamber pressure in a disk-shaped combustor. Proc Combust Inst 2017;36:2673–80. https://doi.org/10.1016/j.proci.2016.07.097.
[44] Kawasaki A, Inakawa T, Kasahara J, Goto K, Matsuoka K, Matsuo A, Funaki I. Critical condition of inner cylinder radius for sustaining rotating detonation waves in rotating detonation engine thruster. Proc Combust Inst 2019;37:3461–9. https://doi.org/10.1016/j.proci.2018.07.070.
[45] Yokoo R, Goto K, Kasahara J, Athmanathan V, Braun J, Paniagua G, Meyer TR, Kawasaki A, Matsuoka K, Matsuo A, Funaki I. Experimental study of internal flow structures in cylindrical rotating detonation engines. Proc Combust Inst 2021;38:3759–68. https://doi.org/10.1016/j.proci.2020.08.001.
[46] Prakash S, Raman V, Lietz CF, Hargus WA, Schumaker SA. Numerical simulation of a methane-oxygen rotating detonation rocket engine. Proc Combust Inst 2021;38:3777–86. https://doi.org/10.1016/j.proci.2020.06.288.
[47] Conaire MO, Curran HJ, Simmie JCM, Pitz WJ, Westbrook CK. A comprehensive modeling study of hydrogen oxidation. Int J Chem Kinet 2004;36:603–22. https://doi.org/10.1002/kin.20036.

[48] Marcantoni LFG, Elaskar S, Tamagno J, Saldía J, Krause G. An assessment of the openfoam implementation of the knp scheme to simulate strong explosions. Shock Waves 2021;31:193–202. https://doi.org/10.1007/s00193-021-01008-8.
[49] Kurganov A, Noelle S, Petrova G. Semidiscrete central-upwind schemes for hyperbolic conservation laws and Hamilton-Jacobi equations. SIAM J Sci Comput 2001;23:707–40. https://doi.org/10.1137/S1064827500373413.
[50] Bram VL. Flux-vector splitting for the euler equation. Springer Berlin Heidelberg; 1997. p. 80–9.
[51] Burke RF, Rezzag T, Ahmed K. Carbon and hydrocarbon particle seeding in air-breathing rotating detonation engine. J Eng Gas Turbines Power 2022;144. https://doi.org/10.1115/1.4051987.
[52] Meng Q, Zhao M, Zheng H, Zhang H. Eulerian-Lagrangian modelling of rotating detonative combustion in partially pre-vaporized n-heptane sprays with hydrogen addition. Fuel 2021;290:119808. https://doi.org/10.1016/j.fuel.2020.119808.
[53] Tang-Yuk KC, Mi X, Lee JHS, Ng HD, Deiterding R. Transmission of a detonation wave across an inert layer. Combust Flame 2022;236:111769. https://doi.org/10.1016/j.combustflame.2021.111769.
[54] Wang Y, Huang C, Deiterding R, Chen H, Chen Z. Propagation of gaseous detonation across inert layers. Proc Combust Inst 2021;38:3555–63. https://doi.org/10.1016/j.proci.2020.07.022.
[55] Ng HD, Radulescu MI, Higgins AJ, Nikiforakis N, Lee JHS. Numerical investigation of the instability for one-dimensional chapman–jouguet detonations with chain-branching kinetics. Combust Theor Model 2005;9:385–401. https://doi.org/10.1080/13647830500307758.